Materials Science & Engineering A 631 (2015) 209–213

Contents lists available at ScienceDirect

Materials Science & Engineering A

journal homepage: www.elsevier.com/locate/msea

On the effects of the Mg content on the critical strain for the jerky flow of Al–Mg alloys

H. Ait-Amokhtar [a,*], C. Fressengeas [b], K. Bouabdallah [c]

[a] Laboratoire de Physico-Chimie des Matériaux et Catalyse (LPCMC), Faculté des Sciences Exactes, Université de Bejaia, 06000 Bejaia, Algeria
[b] Laboratoire d'Etude des Microstructures et de Mécanique des Matériaux (LEM3), Université de Lorraine/CNRS, Ile du Saulcy, 57045 Metz Cedex, France
[c] Faculté de Technologie, Université de M'sila, 28000 M'sila, Algeria

ARTICLE INFO

Article history:
Received 21 November 2014
Received in revised form
17 February 2015
Accepted 19 February 2015
Available online 2 March 2015

Keywords:
Al–Mg alloys
Jerky flow
Dynamic strain aging
Portevin–Le Chatelier effect
Critical strain

ABSTRACT

The jerky flow of Al–Mg alloys is investigated during tensile tests at imposed strain rate and room temperature. The strain and strain rate dependences of the magnitude of the stress drops, the range of plastic instability and the critical strain for the onset of serrations are studied in connection with the Mg content. In the low strain rate part of the strain rate range of instability, the critical strain decreases with the Mg content. The critical strain rate corresponding to the minimum of the critical strain vs. applied strain rate curve shifts to larger values when the Mg content increases. This behavior leads to an enlargement of the strain rate domain of inverse behavior of the critical strain, at the expense of the domain of normal behavior. In the high strain rate part of the range of instability, the critical strain does not depend on the Mg content. These results are discussed in accordance with dynamic strain aging mechanisms.

1. Introduction

It is well established that the jerky flow of alloys or the Portevin–Le Chatelier (PLC) effect originates in dynamic strain aging (DSA), i.e., a dynamic interaction between solute atoms and mobile dislocations: the solute atoms diffuse to and pin mobile dislocations during their temporary arrest at local obstacles (forest dislocations, precipitates, etc.) [1–3]. Two diffusion mechanisms have been considered to substantiate DSA. In the first one, it is assumed that solute atmospheres form by bulk diffusion around mobile dislocations during their temporary arrests at obstacles. Such a mechanism is enhanced by the nucleation of vacancies during deformation [4,5]. In the second mechanism, referred to as pipe-diffusion, solute atmospheres first form around forest dislocations, before solute atoms diffuse along their lines toward mobile dislocations during their waiting time [6–9]. The diffusion of solute atoms toward mobile or forest dislocations has distinct effects on plasticity. Diffusion to mobile dislocations directly affects plasticity and the PLC phenomenon by modulating the motion of these dislocations. Diffusion towards forest dislocations contributes to hardening by raising the strength of the obstacles to dislocation motion, which only indirectly influences plasticity. The additional pinning of dislocations becomes more efficient and the overcoming of obstacles more difficult when the waiting time increases, i.e. when the applied strain rate decreases, at the opposite of the "normal" thermal activation trend. The strain rate sensitivity (SRS) of the flow stress may therefore become negative if, in a certain range of plastic strain, strain rate and temperature, the solute atoms and dislocations have comparable mobility. Negative SRS and the elastic interactions responsible for the spatial coupling of dislocations lead to their repeated collective breakaway from solute clouds and to strain localization into narrow bands, which results in serrated stress–strain curves at constant applied strain rate [10–18].

Three types of PLC deformation bands, associated to three distinct kinds of strain localization, have been commonly reported at constant applied strain rate [13–17]. At very low strain rates, type C static bands appear randomly on the sample surface, due to weak spatial coupling between plasticity events, and produce large drops on the stress–strain curves. Type A bands appear at large strain rates and produce weak undulations on the stress–strain curves. They are characterized by continuous propagation due to strong spatial coupling of dislocation ensembles. At intermediate strain rates, marginal spatial coupling gives rise to type B hopping bands (apparent propagation) and to regular stress drops on the stress–strain curve. There is an increasing propensity to propagation with increasing applied strain rate and/or decreasing temperature.

* Corresponding author. Tel.: +213 662 17 88 15; fax: +213 34 21 59 86.
E-mail address: aitamokhtar_h@yahoo.fr (H. Ait-Amokhtar).

http://dx.doi.org/10.1016/j.msea.2015.02.055
0921-5093/

For an imposed strain rate $\dot{\varepsilon}_a$, the uniform tensile plastic flow becomes unstable beyond a certain critical plastic strain ε_c and, usually, remains such until failure by necking of the sample. At a prescribed temperature, ε_c first decreases, then increases when the applied strain rate $\dot{\varepsilon}_a$ increases [14,19,20]. The descending branch of the curve $\varepsilon_c(\dot{\varepsilon}_a)$ reflects "inverse" behavior (meaning that such behavior is *a priori* not expected from a thermally activated mechanism), and corresponds to types C and B bands. In this strain rate sub-domain, the bands can also switch from type B to type C with increasing strain [14]. The ascending branch of the curve $\varepsilon_c(\dot{\varepsilon}_a)$, reflects "normal" behavior, and corresponds to instabilities of type A. In the strain rate range where the behavior of the critical strain switches from "inverse" to "normal", instabilities shift from type A to type B with increasing strain [14,19,21]. As suggested above, the normal behavior is well explained by DSA models [3,4], but the inverse behavior is still a matter of controversy. In a plausible interpretation, to be developed in what follows, inverse behavior has been associated with large initial densities of mobile dislocations while low densities have been seen as promoting normal behavior [22].

In Al–Mg alloys, several studies have shown that Mg is the solute element responsible for DSA [8,23–25]. Indeed, the Mg content significantly affects jerky flow characteristics such as the range of instability, the magnitude of the stress drops or the reloading time between two successive stress drops. However, with the exception of [14], there are very few studies devoted to the dependence of the critical strain on the Mg content, particularly in the inverse behavior range of strain rates. In the present work, we study jerky flow in five Al–Mg alloys with different Mg contents during tensile tests at imposed strain rate and at room temperature. We analyze the effects of the Mg content on the size of the stress drops and on the critical strain for instability when the applied strain rate is varied. These effects are discussed in relation with the diffusion of Mg atoms and the DSA mechanism.

2. Experimental procedure

Five Al–Mg alloys of different Mg content were used in this study. Their chemical composition in weight percent are given in Table 1.

Polycrystalline flat samples were machined in the rolling direction and deformed in tension at room temperature with a hard testing machine (i.e., with constant driving velocity) at strain rates in the range 10^{-6}–10^{-1} s^{-1}. Due to DSA, the uniform tensile plastic flow is unstable in these conditions. The resulting PLC bands and their spatiotemporal aspects were studied in earlier reports, using in particular white light interferometry [14,26], digital image correlation [16,21,26] and infrared thermography [21,26,27].

Table 1
Chemical compositions of the Al–Mg alloys (in wt%).

Alloy	Mg	Mn	Si	Fe	Cu	Zn	Ti	Cr
Al–1%Mg	0.904	1.086	0.200	0.488	0.027	0.005	0.012	0.015
Al–2%Mg	1.998	0.079	0.098	0.270	0.020	0.006	0.016	0.194
Al–2.5%Mg	2.606	0.028	0.125	0.199	0.070	0.010	0.008	0.210
Al–3.2%Mg	3.218	0.475	0.165	0.296	0.055	0.043	0.035	0.094
Al–4.5%Mg	4.448	0.421	0.400	0.413	0.10	0.250	0.148	0.053

3. Results and discussion

3.1. Stress vs. strain curves and magnitude of the stress drops

For an imposed strain rate ranging from 10^{-6} to 10^{-1} s^{-1}, the uniform tensile plastic flow of the investigated alloys becomes unstable beyond a certain critical plastic strain and remains such until failure by necking of the sample. At a given strain, the flow stress decreases when the strain rate increases, i.e. the SRS is negative. The average value of the SRS, calculated between two strain rates, decreases with strain, which suggests that DSA is favored by further straining. In what follows, both true strain and engineering strain are used in analyzing deformation curves. Fig. 1 shows serrated stress–strain curves in Al–2%Mg, Al–2.5%Mg, Al–3.2%Mg and Al–4.5%Mg alloys at the same applied strain rate of 2.38×10^{-4} s^{-1}. The figure suggests that jerky flow is strongly influenced by the Mg content, as show the shift of the critical strain and the increase of the stress drop size when it increases.

The size $\Delta\sigma$ of the stress drops is one of the most conspicuous characteristics of the PLC instabilities. It reveals the degree of heterogeneity of the plastic flow. Indeed, the deformation becomes more heterogeneous as $\Delta\sigma$ increases [8,14,15]. Before studying the effect of the Mg content on $\Delta\sigma$, we examine the strain and strain rate dependence of the latter. Fig. 2 depicts its strain dependence in the Al–3.2%Mg alloy for various strain rates. The figure shows that $\Delta\sigma$ increases with strain and decreases with increasing strain rate. Similar results were obtained in the Al–2% Mg, Al–2.5%Mg and Al–4.5%Mg alloys [14], and confirmed by the weak type A undulations observed in an Al–1%Mg alloy [26]. The strain rate dependence of the stress drop size can be cast into the power law form:

$$\Delta\sigma \propto \dot{\varepsilon}^{-\lambda} \tag{1}$$

The exponent λ is weakly dependent on strain and on the Mg content, and it is almost constant and close to 1/3. This result agrees with those of Ling and McCormick [7], Pink and Grinberg [8] and Schwink and Nortmann [9]. This value corresponds to the pipe diffusion of solute Mg atoms through forest dislocation cores. In the Cottrell–Bilby law [5], which provides the concentration of the solute atoms moving towards dislocations by bulk diffusion, the exponent is given the value $\lambda = 2/3$. In all the alloys of the present study, λ is much closer to 1/3 than 2/3. This result suggests

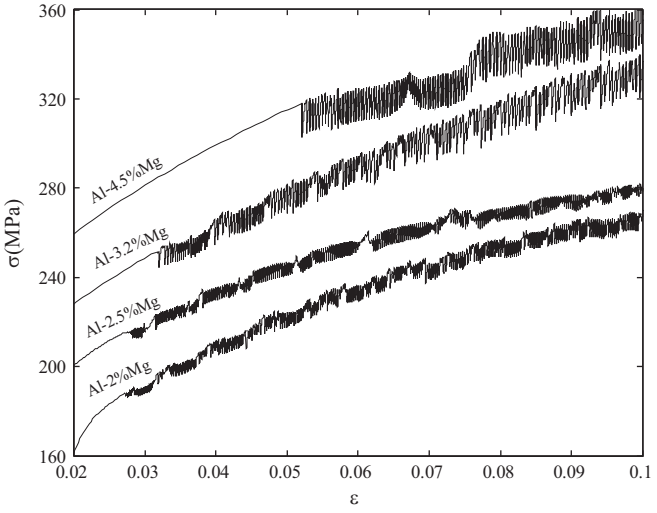

Fig. 1. Serrated stress–strain curves at strain rate 2.38×10^{-4} s^{-1} for various Al–Mg alloys at room temperature. For a better view, the curve of the Al–4.5%Mg alloy is shifted downwards by 50 MPa and the curve of the Al–3.2%Mg alloy is shifted upwards by 40 MPa.

that pipe diffusion is more relevant than bulk diffusion in our experiments.

For a given applied strain rate, the evolution with the strain ε of the stress drop size $\Delta\sigma$ can be approximated by a power law [8,12]

$$\Delta\sigma \propto \varepsilon^{\theta} \tag{2}$$

where the exponent θ depends on the applied strain rate and Mg content. The evolution of θ with strain rate is plotted in Fig. 3 for four alloys and for an Al–5%Mg alloy studied by Pink and Grinberg [8]. The figure clearly shows that the exponent θ increases with the applied strain rate and Mg content.

The above effects of strain, strain rate and Mg content on $\Delta\sigma$ can be explained by the standard model of DSA, in a version recently used in the reference [28]. In this paper, the waiting time t_w of dislocations at local obstacles is written as

$$t_w = \frac{\rho_f^{-1/2}}{V} \tag{3}$$

where ρ_f is the forest dislocation density, $\rho_f^{-1/2}$ the mean free path of mobile dislocations between forest obstacles and V the dislocation velocity. An Arrhenius dependence is assumed for the latter, in the form:

$$V = V_0 \exp\left(\frac{\sigma - \sigma_h - \sigma_s}{S_0}\right) \tag{4}$$

Here, V_0 is a reference velocity, S_0 is the SRS of the flow stress in the absence of solute effects, σ_h the Taylor (forest) hardening stress and σ_s the additional pinning stress due to aging. In turn, V_0 can be written as: $V_0 = \upsilon_0 \rho_f^{-1/2}$, where υ_0 is a constant reference frequency for dislocation unpinning. The Taylor hardening stress is taken in the Bayley–Hirsch form:

$$\sigma_h = \alpha \mu b \rho_f^{1/2} \tag{5}$$

where α is a constant, μ the shear modulus and b the Burgers vector modulus. Following Louat [29] the pinning stress is written as:

$$\sigma_s = f_0(1 - \exp(-(t_a/\tau)^{1/3}) \tag{6}$$

where t_a denotes the aging time, τ is the characteristic time for solute diffusivity and f_0 represents the pinning stress at saturation, an increasing function of the Mg content. As already suggested above, the exponent 1/3 stands for pipe diffusion. From Eqs. (3), (4),(6), the chain differentiation rule provides the variation of the waiting time t_w with f_0, and consequently with the Mg content:

$$\frac{\partial t_w}{\partial f_0} = \frac{\partial t_w}{\partial V}\frac{\partial V}{\partial \sigma_s}\frac{\partial \sigma_s}{\partial f_0} = \frac{\rho_f^{-1/2}\sigma_s}{V S_0 f_0} > 0 \tag{7}$$

all other factors being held constant.[1] As it is positive, the waiting time increases with the Mg content, which allows more time for diffusion. Hence, the pinning stress becomes larger, not only because its saturated value becomes larger, but also because large values are reached more easily during the waiting time. Consequently, DSA becomes more efficient and the size of the stress drops becomes larger. This effect is similar to that taking place when the applied strain rate is decreased in the range of instability. Note also that the waiting time is strongly stress-dependent during a single test, which generates unsteadiness of the deformation process. In particular, the chain differentiation rule applied to Eqs. (3)–(5) provides the variation of the waiting time with the forest dislocation density

$$\frac{\partial t_w}{\partial \rho_f} = \frac{\partial t_w}{\partial V}\frac{\partial V}{\partial \sigma_h}\frac{\partial \sigma_h}{\partial \rho_f} = \frac{1}{2}\frac{t_w}{\rho_f}\left(\frac{\sigma_h}{S_0} - 1\right) \tag{8}$$

all other factors being held constant. Considering $\alpha = 0.7$, $\mu = 28.5$ GPa, $b = 0.286$ nm, $\rho_f = 10^{13}$ m^{-2} and $S_0 = 3$ MPa [31–33], and assuming that the mobile density increases with increasing forest density, a plausible assumption in monotonous loading, Eq. (8) shows that the waiting time increases with increasing mobile dislocation density. Again, this is more time allowed for the diffusion of solute atoms towards arrested dislocations, larger stress drops and a more efficient DSA.

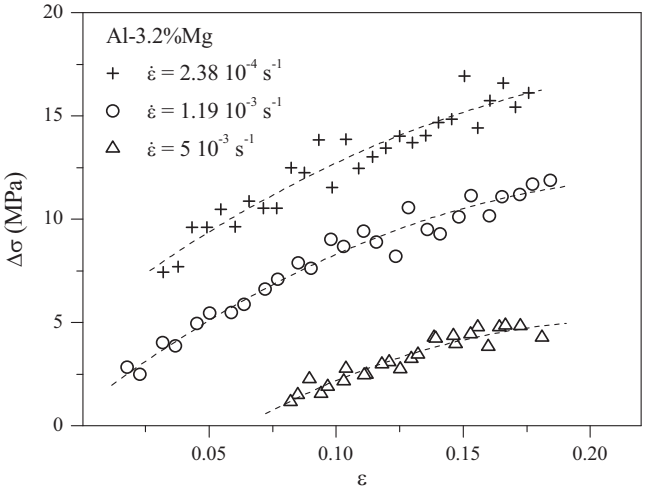

Fig. 2. Strain dependence of the magnitude of the stress drops at room temperature and at various strain rates in the Al–3.2%Mg.

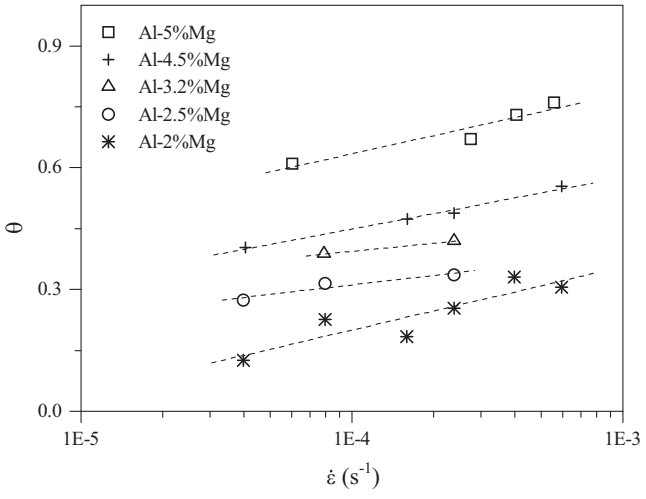

Fig. 3. Strain rate and Mg content dependences of the parameter θ, comparison with Pink and Grinberg [8] results in the Al–5%Mg alloy.

3.2. Effects of Mg content on the domain of instability and on the critical strain

As already mentioned, the uniform tensile plastic flow becomes unstable beyond a certain strain rate-dependent critical strain ε_C. Fig. 4 shows an example of serrated stress–strain curves in the Al–3.2%Mg alloy at the applied strain rates of 2.38×10^{-4} s^{-1}, 5×10^{-3} s^{-1} and 5×10^{-2} s^{-1}. The dependence of ε_C on the imposed strain rate was studied in several earlier papers [12,14,20–21], with the following results. At low strain rates, ε_C

[1] Note that the time derivative of the aging time dynamics may depend on the waiting time, as in McCormick model [30]. However, this does not imply a one-to-one correspondence between aging time and waiting time.

shows inverse behavior and the band type is C or B. At a certain critical strain rate $\dot{\varepsilon}_C$, the behavior switches from "inverse" to "normal", and the band type switches from C-B to A. $\dot{\varepsilon}_C$ is the strain rate leading to the lowest critical strain in the strain rate range for instability. It correlates with the gradual change of the PLC bands from continuous propagation (type A) to intermittent progression (type B) with increasing strain. This crossover was thoroughly studied in the Al–3.2%Mg alloy using infrared thermography [21]. In addition, we observed some correlation between the plastic strain at failure ε_r and the critical plastic strain ε_C when the strain rate is varied [14].

Fig. 5 shows the strain rare dependence of the critical strain for the studied alloys with different Mg content. We show in particular that ε_C decreases with decreasing Mg content at low applied strain rates, and that it is weakly dependent on this quantity at high strain rates. Thus, the strain range of instability increases if the Mg content is decreased, which may seem paradoxical. Independently but similarly, Balík et al. [22] showed that the critical strain decreases with the initial mobile dislocations density at low applied strain rates. Indeed, at such strain rates, when the initial mobile density is large, the critical strain is large and it shows inverse behavior. When this density is lowered by an appropriate treatment, the critical strain is low and it shows normal behavior. Thus, the range of instability increases if the initial mobile dislocations density is decreased. A unified explanation for these two similar trends can be given by considering the parallel influences of the dislocation density and Mg content on the effectiveness of pipe diffusion. At a low strain rate in the range of instability, ample time is available for diffusion, particularly when the Mg content and the dislocation density are large, as shown above. In such a situation, the saturation level of the pinning stress is reached quickly during the waiting time. Therefore, stress drops cannot take place, which implies that instability is delayed to larger strains, i.e. the critical strain tends to be larger. Clearly, pipe diffusion is less effective if the applied strain rate is slightly increased from the chosen value. Therefore, inverse behavior of the critical strain can be expected. Conversely, the waiting time decreases if the dislocation density and/or the Mg content are low. Then the diffusion is less effective and, although the SRS is still negative, the saturation level of the pinning stress may not be reached during aging, even at low applied strain rates. Such a situation gives rise to unstable plastic flow at small strains, and therefore to low critical strains. It may be such that the inverse behavior of the critical strain is impeded, as observed in [22] when the dislocation density is maintained at a low level.

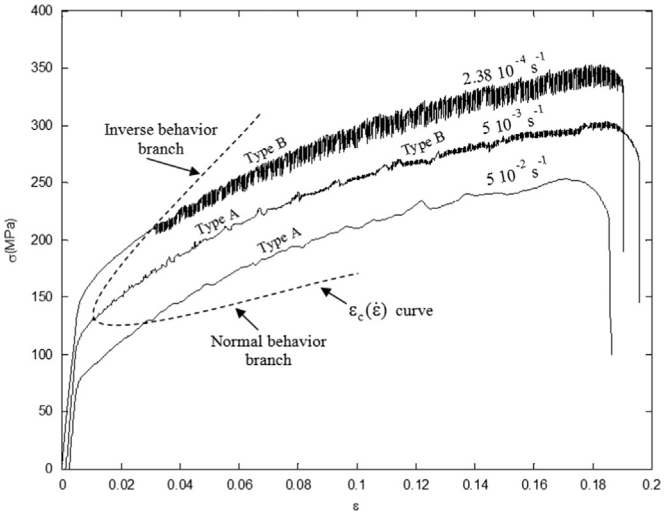

Fig. 4. Serrated stress–strain curves in the Al–3.2%Mg alloy, at various applied strain rates, showing the critical strain switch from "inverse" to "normal" behavior when the applied strain rate increases. For a better view, curves at 5×10^{-3} s^{-1} and at 5×10^{-2} s^{-1} are shifted downwards by 40 MPa and 80 MPa respectively.

For reasons of continuity of the curve $\varepsilon_C(\dot{\varepsilon}_a)$, increasing the Mg content has also consequences on the critical strain rate $\dot{\varepsilon}_C$ where the behavior of the critical strain switches from inverse to normal. The dependence of $\dot{\varepsilon}_C$ on the Mg content is depicted in Fig. 6. The figure shows that $\dot{\varepsilon}_C$ shifts to higher values when the Mg content increases, which amounts to enlarging the inverse behavior range at the expense of the normal behavior range. This result is in agreement with those obtained from the experimental curves $\varepsilon_C(\dot{\varepsilon}_a)$ reported by Král and Lukáč [19] in Al–2.6%Mg and Al–4.8%Mg alloys, and by Chihab and Fressengeas [34] in Al–0.9%Mg and Al–2%Mg alloys. The shift of $\dot{\varepsilon}_C$ as a function of the Mg content can be interpreted as follows. Let C_1, $C_2 > C_1$ be two Mg concentrations, and let $\dot{\varepsilon}_{C1}$ be the critical strain rate for the concentration C_1. Consider a strain rate $\dot{\varepsilon}$, equal or slightly larger than $\dot{\varepsilon}_{C1}$: $\dot{\varepsilon} \geq \dot{\varepsilon}_{C1}$, and the positive increment of strain rate $d\dot{\varepsilon}$: $\dot{\varepsilon}+d\dot{\varepsilon} > \dot{\varepsilon}$. In this increment, the waiting time decreases by the amount $dt_{W\dot{\varepsilon}} < 0$ and the critical strain increases by $d\varepsilon_C > 0$. Now, consider the alloy with Mg content C_2, everything else being equal. At strain rate $\dot{\varepsilon}$, the increment $d\dot{\varepsilon}$ now entails a variation dt_W of the waiting time such that: $dt_W = dt_{W\dot{\varepsilon}} + dt_{WC} > 0$ with $dt_{W\dot{\varepsilon}} < 0$ and $dt_{WC} > 0$, with the consequence $d\varepsilon_C < 0$ because the positive variation of the waiting time $dt_{WC} > 0$ due to the Mg content increase is larger (in absolute value) than the negative variation $dt_{W\dot{\varepsilon}} < 0$ arising from

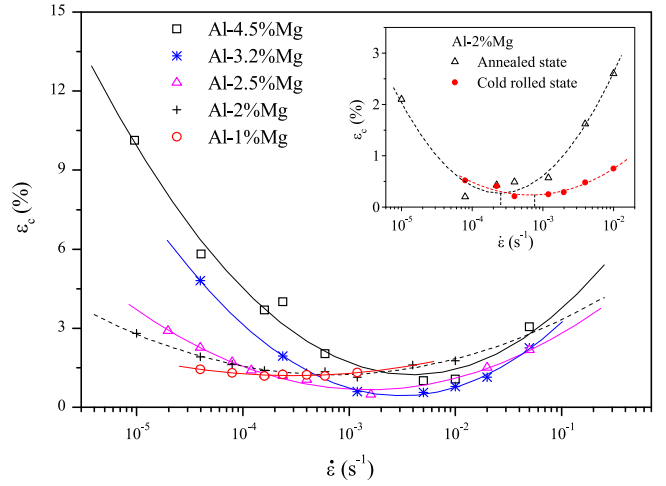

Fig. 5. Applied strain rate dependence of the critical plastic strain for different Al–Mg alloys. Inset: effect of heat treatment (annealing at 400 °C for 2 h) on the critical strain in the Al–2%Mg, according to Ziani et al. [20].

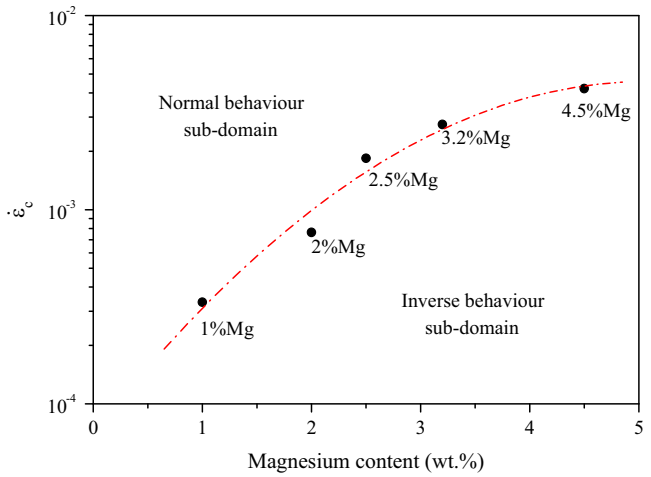

Fig. 6. Effect of the nominal concentration of Mg on $\dot{\varepsilon}_C$, the minimum of the curve $\varepsilon_C(\dot{\varepsilon})$.

the increase of strain rate. Hence, the behavior of the critical strain ε_C switches from normal to inverse at the strain rate $\dot{\varepsilon}$ when C_1 is changed into $C_2 > C_1$.

Similar behavior of the critical strain and of the critical strain rate can be obtained by controlling the initial mobile dislocation density. Indeed, we observed from the curves $\varepsilon_C(\dot{\varepsilon})$ obtained in the Al–2%Mg alloy in cold-rolled and annealed states that ε_C is smaller in the descending part of the curve, and that $\dot{\varepsilon}_C$ has a smaller value, in the annealed state [20]. Our measurements indicate that the internal stresses are less significant in the latter state, as could be expected, and that the dislocation density is lower (see Fig. 2 in [20]). According to the above analysis, the waiting time is therefore smaller at low strain rates in the annealed state, which induces a smaller a critical strain as well as a smaller critical strain rate, as indicated in the inset of Fig. 5.

3.3. Effects of Mg content on the band type

Increasing the Mg content has effects on the observed band type at a given imposed strain rate. For example, at the strain rate $2 \times 10^{-3}\,s^{-1}$, the band type is A in Al–1%Mg and Al–2%Mg alloys and B in Al–3.2%Mg and Al–4.5%Mg alloys. Our interpretation of this phenomenon is as follows. As shown above, the waiting time increases with the Mg content, and the diffusion of Mg atoms becomes more effective, which favors DSA. Therefore, the size of the stress drops increases, as well as the reloading time between drops. Thus, there is more time for the plastic relaxation of the internal stresses arising from the heterogeneity of strain in the vicinity of the bands, and less of the coupling forces they induce. Since discontinuous propagation (type B) requires less spatial coupling than continuous propagation (type A) [11–15], this evolution in the microstructure favors a switch of the band type from type A to type B. Note that a similar interpretation, albeit deriving from the intrinsic unsteadiness of the tensile test, was provided in [21] to explain the crossover from type A to type B in the course of a single test.

4. Conclusion

In the present paper, we studied several characteristics of the jerky flow arising in Al–Mg alloys during velocity driven tensile tests at room temperature, in connection with the Mg content of the alloys. It was shown that increasing the Mg concentration strongly affects the size of the stress drops, the critical strain for the onset of serrations, the strain and strain rate range of instability and the type of the instability.

DSA becomes more efficient when the Mg content increases because the saturation level of the pinning stress increases. In addition, the waiting time of mobile dislocations on their obstacles increases, which enhances the diffusion of Mg atoms toward dislocations at low applied strain rates. Therefore, the Mg content controls the occurrence of the critical strain for the onset of instability in this range of applied strain rates. Indeed, the critical strain decreases with the Mg content.

For the same reasons, the critical strain rate $\dot{\varepsilon}_C$ corresponding to the transition between inverse and normal behavior of ε_C shifts to larger values of strain rate when the Mg content increases, which amounts to expending the inverse behavior sub-domain at the expense of the normal behavior sub-domain. The critical strain is not affected by the Mg content at high strain rates, because it is controlled by a lack of diffusivity in this range.

In complement, we emphasized the role of the initial mobile dislocation density in controlling the waiting time and the critical strain at low applied strain rates. These results suggest that accounting for the unsteadiness of diffusivity is essential for the prediction of the critical strain for instability. Recent DSA models [35,36] demonstrating some success in this respect actually based their formalism on such ideas.

Acknowledgments

H. A.-A. is thankful to University of Bejaia (Algeria) for financial support and the people in charge of LEM3 (University of Lorraine/CNRS, France) for their welcome and help.

References

[1] C. Fressengeas, A.J. Beaudoin, M. Lebyodkin, L.P. Kubin, Y. Estrin, Mater. Sci. Eng. A 400–401 (2005) 226.
[2] L.P. Kubin, C. Fressengeas, G. Ananthakrishna, Collective behaviour of dislocations in plasticity, in: F.R.N. Nabarro, M.S. Duesbery (Eds.), Dislocations in Solids, vol. 11, Elsevier Science BV, Amsterdam, 2002, pp. 101–192.
[3] A. Van den Beukel, Phys. Status Solidi A 30 (1975) 197.
[4] P.G. McCormick, Acta Metall. 20 (1972) 351.
[5] H. Cottrell, B.A. Bilby, Proc. R. Soc. Lond. B 62 (1949) 229.
[6] F.B. Klose, A. Ziegenbein, F. Hagemanna, H. Neuhäuser, P. Hähner, M. Abbadi, A. Zeghloul, Mater. Sci. Eng. A 369 (2004) 76.
[7] C.P. Ling, P.G. McCormick, Acta Metall. Mater. 41 (1993) 3127.
[8] E. Pink, A. Grinberg, Acta Metall. 30 (1982) 2153.
[9] Ch. Schwink, A. Nortmann, Mater. Sci. Eng. A 234–236 (1997) 1.
[10] L.P. Kubin, Y. Estrin, J. Phys. III 1 (1991) 929.
[11] R.A. Mulford, U.F. Kocks, Acta Metall. 27 (1979) 1125.
[12] K. Chihab, H. Ait-Amokhtar, K. Bouabdellah, Ann. Chim. Sci. Matér. 27 (2002) 69.
[13] Y. Estrin, L.P. Kubin, Continuum Models for Materials with Microstructure, Edited by H.-B. Mühlhaus, 1995, pp. 395–450.
[14] H. Ait-Amokhtar, S. Boudrahem, C. Fressengeas, Scr. Mater. 54 (2006) 2113.
[15] S. Kok, M.S. Bharathi, A.J. Beaudoin, C. Fressengeas, G. Ananthakrishna, L.P. Kubin, M. Lebyodkin, Acta Mater. 51 (2003) 3651.
[16] H. Ait-Amokhtar, P. Vacher, S. Boudrahem, Acta Mater. 54 (2006) 4365.
[17] H. Louche, K. Bouabdallah, P. Vacher, T. Coudert, P. Balland, Exp. Mech. 48 (2008) 714.
[18] S. Fu, T. Cheg, Q. Zhag, Q. Hu, P. Cao, Acta Mater. 60 (2012) 6650.
[19] R. Král, P. Lukáč, Mater. Sci. Eng. A 234–236 (1997) 786.
[20] L. Ziani, S. Boudrahem, H. Ait-Amokhtar, M. Mehenni, B. Kedjar, Mater. Sci. Eng. A 536 (2012) 239.
[21] H. Ait-Amokhtar, C. Fressengeas, Acta Mater. 58 (2010) 1342.
[22] J. Balík, P. Lukác, L.P. Kubin, Scr. Mater. 42 (2000) 465.
[23] T. Tabata, H. Fugita, Y. Nakajima, Acta Metall. 28 (1980) 795.
[24] J.M. Robinson, Mater. Sci. Eng. A 203 (1995) 238.
[25] G.G. Saha, P.G. McCormick, P. Rama Rao, Mater. Sci. Eng. 62 (1984) 187.
[26] H. Ait-Amokhtar, Thèse de Doctorat, Université de Bejaia, Algérie, 2006.
[27] H. Ait-Amokhtar, C. Fressengeas, S. Boudrahem, Mater. Sci. Eng. A 488 (2008) 540.
[28] V. Taupin, S. Varadhan, C. Fressengeas, A.J. Beaudoin, Acta Mater. 56 (2008) 3002.
[29] N. Louat, Scr. Metall. 15 (1981) 1167.
[30] P.G. McCormick, Acta Metall. 36 (1988) 3061.
[31] H. Gao, Y. Huang, Int. J. Solids Struct. 38 (2001) 2615.
[32] G. Horvath, N.Q. Chinh, J. Gubicza, J. Lendvai, Mater. Sci. Eng. A 445–446 (2007) 186.
[33] L.P. Kubin, Y. Estrin, Acta Metall. Mater. 38 (1990) 697.
[34] K. Chihab, C. Fressengeas, Mater. Sci. Eng. A 356 (2003) 102.
[35] T. Böhlke, G. Bundar, Y. Estrin, M. Lebyodkin, Comput. Mater. Sci. 44 (2009) 1076.
[36] M. Maziere, H. Dierke, Comput. Mater. Sci. 52 (2012) 68.